REGULAR ARTICLE

Polymer Journal

Trivalent Metal Adsorption Properties on Synthesized Viscose Rayon Succinate

By Aruukhan Dashkhuu KHASBAATAR,[1] Yong Jin CHUN,[2] and Ung Su CHOI[1,]*

A viscose rayon succinate (VRS) was synthesized using viscose rayon, succinic anhydride and DMSO. The VRS was well characterized by C^{13} nuclear magnetic resonance, Fourier transform infrared analysis and properties of the VRS up taking trivalent metals from aqueous solution were investigated. Both esterification and carboxyl bonding of the VRS were assigned essentially at 1729 and 1693 cm^{-1}, respectively. And the essential band of bonding between metal and the material was determined at 1605–1639 cm^{-1}. The available adsorption capacity, degree of substitution and p*K*a of the VRS were 6.2 mequiv/g, 2.5 and 3.72, respectively. The adsorption of metal ions on the VRS follows the order of $Cr^{3+} > Al^{3+} > Fe^{3+}$ with maximum adsorptions capacities 1.48, 1.059 and 1.029 mmol/g. An equilibrium modeling, which is obtained from chemical potential and Boltzmann distribution, was demonstrated trivalent metal adsorption on the VRS in different pHs. Surface potential, Ψ_0, an effective ratio of surface equilibrium constants, K_{effect}, the probability factor $P(A)$ and a degree of protonation, χ represent the physicochemical interactions between carboxyl group and metal ions.

KEY WORDS: Chelating Fiber / Viscose Rayon / Metal Adsorption / Carboxyl Group / FT-IR / Adsorption Modeling /

Fibers have been used in many applications due to their advantages and properties such as high adsorption capacity, and good electrical conductivity.[1] A fiber type of viscose rayon (VR) is a kind of regenerated cellulose which is abundant and easily accessible biopolymer probably suitable for developing novel type of materials with various advanced functions.[2] The most known method of modification of cellulose is esterification that can increase a number of applications. Also, inorganic and organic esters of cellulose played an important role in coating applications.[3]

Some cellulose esters which functional groups have been introduced into them, have been employed successfully in some areas such as removal of harmful trace metal ions, because of their highly selective adsorptivity for heavy metal ions.[4] Trivalent heavy metal ions (THM) such as Al^{3+}, Cr^{3+}, and Fe^{3+} in aqueous solution are toxic to all living organisms including human beings, microbes, plants, fish, and mammals.[5–7] Especially, the toxicity Al^{3+} in drinking is well reported, and its involvement to Alzheimer's disease has been documented.[8,9] Even though Cr^{3+} is an essential nutrient, its oxidation to toxic Cr^{6+} can cause lung cancers and ecological problems.[9,10] In drinking water supplement, iron is a common and troublesome mineral due to the corrosion of iron pipes. This contaminant is often the cause of taste, odor, discoloration, and turbidity problems. Moreover, the issue of the corrosion is more concerned than groundwater contamination.[11] Accordingly, the treatment of heavy metals from wastewater, and soil has been required to reduce the metal concentration to less than that designated values which is in environmental regulations. Various efficient methods and technologies are developed for their removal. One of well known methods is to adsorb heavy metals from aqueous solution using chelating fibers.[12]

The physico-chemical mechanisms involved in metal removal such as physical adsorption, ion-exchange and surface complexation can be investigated to optimize the operating conditions, product development and process design.[13]

The most important environmental factor is pH which influences not only the site dissociation, but also the solution chemistry of the heavy metals: hydrolysis, complexation by organic and/or inorganic ligands, redox reactions and precipitation are strongly influenced by pH and, also the speciation and the adsorption availability of the heavy metals are strongly influenced.[14,15]

The aim of this study is to investigate THM adsorption at different pHs and thermal stability of the VRS coupled with THM (VRS-M). We examined the synthesis and structure of the VRS, the VRS-M using Fourier transform infrared (FT-IR) spectroscopy, ^{13}C solid state nuclear magnetic resonance (NMR), field-emission scanning electron (FE-SEM) microscopy, and thermal properties were examined by thermogravimetric analysis (TGA). Also, adsorption equilibrium of trivalent metal ions (Al^{3+}, Fe^{3+}, and Cr^{3+}) on the VRS was investigated. Then the models were used to describe the experimental isotherms.

EXPERIMENTAL

Materials

The VR felt was purchased from Sechang Chemical Co. (Incheon, Korea,). Succinic anhydride ($C_4H_4O_3$; DaeJung Chemicals & Metals Co., Ltd., Korea; ≥99% pure), dimethylsulfoxide (DMSO) ($(CH_3)_2SO$; DaeJung Chemicals & Metals Co., Korea; ≥99.5%), iron chloride hexahydrate ($AlCl_3 \cdot 6H_2O$; DaeJung Chemicals & Metals Co., Korea; ≥97.9%), chromium

[1]Energy Mechanics Research Center, Korea Institute of Science and Technology, P.O.Box 131, Cheongryang, Seoul 130-650, Korea
[2]Dept. of New Mater. & Appl. Chemistry, Chung Woon University, San 29, Namjang-ri, Hongung-gun 350-701, Korea
*To whom correspondence should be addressed (Tel: +82-2-958-5657, Fax: +82-2-958-5659, E-mail: uschoi@kist.re.kr).

 doi:10.1295/polymj.PJ2007127

Polymer Journal

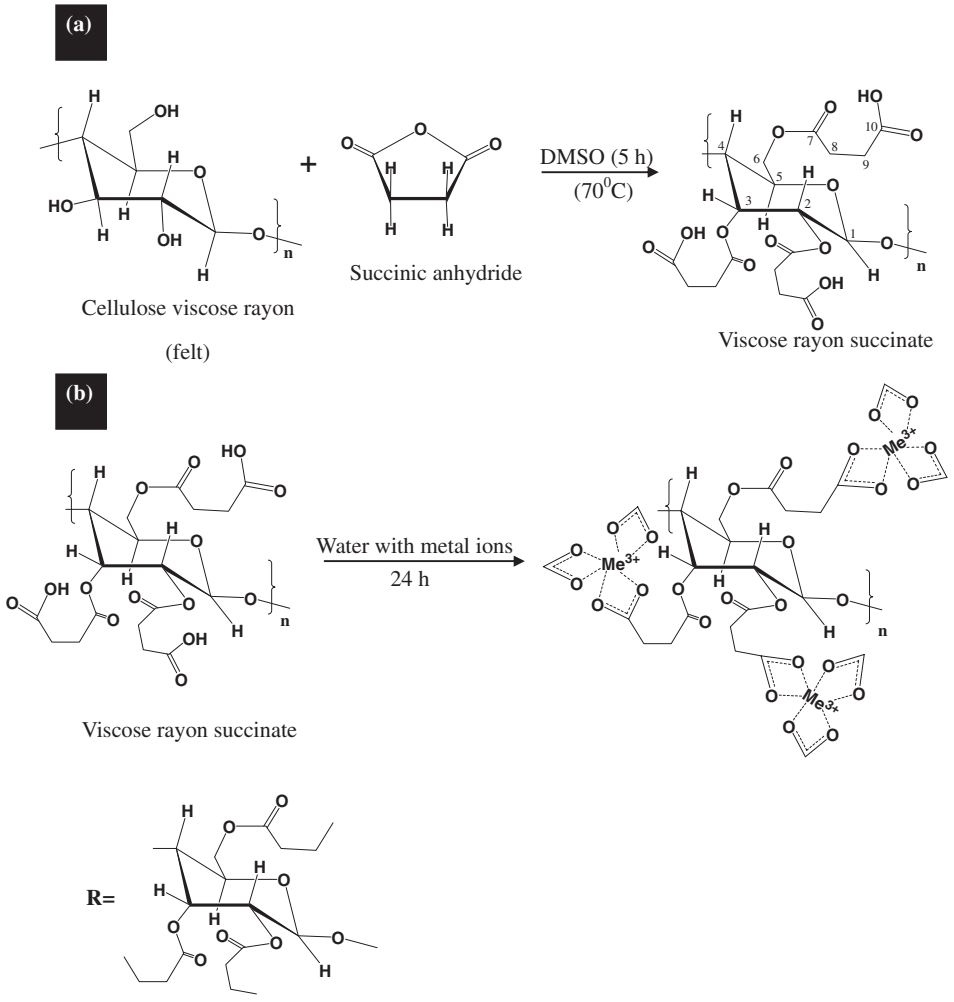

Figure 1. Schematic of synthesizing mechanism of (a) VRS, (b) VRS with metal adsorbed.

chloride hexahydrate ($CrCl_3 \cdot 6H_2O$; Sigma Chemical Co.; ≥99% pure), and aluminum chloride hexahydrate ($AlCl_3 \cdot 6H_2O$; DaeJung Chemicals & Metals Co., Korea; ≥97.9%) were used without further purification. Sigma supplied 0.1 N natrium hydroxide (NaOH), 0.1 N hydrochloric acid (HCl) and 0.1 N nitric acid (HNO_3).

Preparation of the VRS

The VRS was obtained through the heating the VR felt (10 cm × 10 cm, 5 g and 2.8 mm thick) with succinic anhydrate (30 g), and DMSO (500 g) in a round flask with a condenser at 70 °C for 5 h with stirring. The synthesized the VRS was washed with both cold and hot distilled water and dried in a freeze dryer for 24 h. Figure 1(a) shows the chemical structure and the numbering of the carbon atoms of the VRS.

^{13}C NMR (solid state): $\delta = 105$ (C1), 74.8 (C2), 73 (C3), 88 (C4), 90 (C5), 63.5 (C6), 173.8 (C7), 29.9 (C8), 39.8 (C9), and 176 (C10).

Capacity of the VRS

An acid-base titration method was used to determine the cation exchange capacity of the VRS. Exactly 100 mL of 0.1 N NaOH solution were added to a 100 mL Erlenmeyer flask with 0.1 g of the VRS and shaken for 24 h at 200 rpm at room temperature. After being shaken, three 25 mL samples were extracted from the shaken solution and measured using an auto-titrator utilizing a 0.1 N HCl solution. The average value of the cation exchange capacity from the sampled solutions was 6.2 meq/g.

$$\text{R-COOH} + \text{NaOH} \Leftrightarrow \text{R-COONa} + H_2O;$$

$$q_e = \frac{(V_{25} - V_{\text{HCl}})C_{\text{NaOH}}V_{100}}{MV_{25}}$$

Where q_e, is the cation exchange capacity, R is shown in Figure 1, M is the mass of the VRS, V_{100} is the volume of the solution, V_{25} is the volume sampled from the solution, V_{HCl} is the volume of HCl used for back titration, and C_{NaOH} is the initial concentration of NaOH in the solution.

Degree of Substitution (DS) of the VRS

In order to determine the DS of VRS, the same method as obtaining adsorption capacity of VRS was applied. So, ester content was calculated as:

$$\mathrm{EC}(\%) = \frac{(V_{25} - V_{\mathrm{HCl}})C_{\mathrm{NaOH}}M_{\mathrm{sa}}}{10M}$$

where M_{sa} is the molecular weight of grafted succinic residue.

The degree of substitution was then calculated as:

$$\mathrm{DS} = \frac{162\mathrm{EC}}{100M_{\mathrm{sa}} - \mathrm{EC}(M_{\mathrm{sa}} - 1)}$$ [16]

where 162 is the molecular weight of anhydroglucose. The degree of substitution (DS) was 2.5.

p*K*a of the VRS

0.5 g of VRS was protonated by 10 mL of water. Then, it was potentiometrically titrated with 0.1 NaOH using an auto-titrator. The p*K*a was obtained by the well-known equation of Henderson.

$$\mathrm{pH} = \mathrm{p}K\mathrm{a} + \log\frac{[\mathrm{A}^-]}{[\mathrm{HA}]}$$

pH = p*K*a occurs due to the fact that $[\mathrm{A}^-]$ is equal to [HA] at the half-neutralization points.[17] The value of the p*K*a is 3.72.

Quantitative Analysis of the Adsorption of Al^{3+}, Fe^{3+}, and Cr^{3+}

A hundred ml of pH adjusted solutions containing 10 mM each of Al^{3+}, Fe^{3+}, and Cr^{3+}, and 0.1 g of the VRS were placed in Erlenmeyer flasks and shaken for 24 h at 200 rpm. After removed the VRS from the solution, the concentration of metal not removed from the solution was determined by an atomic absorption spectrometer (AAS.) The VRS with metal was dried at 40 °C in a vacuum oven for 24 h and characterized by a FT-IR spectrometer. Concentrated HCl was used to adjust the pHs of the metal ion aqueous solutions.

Measurements

FT-IR spectra (4000–200 cm^{-1}, KBr disc) were recorded on a GX FT-IR PerkinElmer spectrometer. ^{13}C NMR spectra were obtained on a Bruker MSL200 spectrometer in the solid state. The VRS-Al and mapping of aluminum were observed in a FE-SEM (Hitachi S4200) at 15.0 kV. An atomic absorption spectrometer (AAS; SpectraAA 800, Varian, USA) and inductively coupled plasma (ICP) mass spectrometer (Polyscan 61E, Theromo Jarrell Ash) were used for quantitative analyses of the quantitative analysis of adsorbed ions. TGA were carried out with a DuPont 951 thermogravimetric analyzer. The TGA curves were obtained under a nitrogen atmosphere at a flow rate of 4 mL/min and scanning rate of 10 °C/min. The adsorption capacity, DS, p*K*a of the VRS and the pH values were measured using an auto-titrator (Metrohm 728, Switzerland), and pH 300 (Hanna Instruments, Italy) digital pH meter, respectively.

RESULTS AND DISCUSSIONS

Surface Characterization of Modified the VR

FT-IR spectra of the VR, and the VRS are recorded in the 4000 to 500 cm^{-1} region and the characteristic bands are shown in Figure 2(a) and 2(b). The main difference of FT-IR spectra between the VR and the VRS was that bonding effects

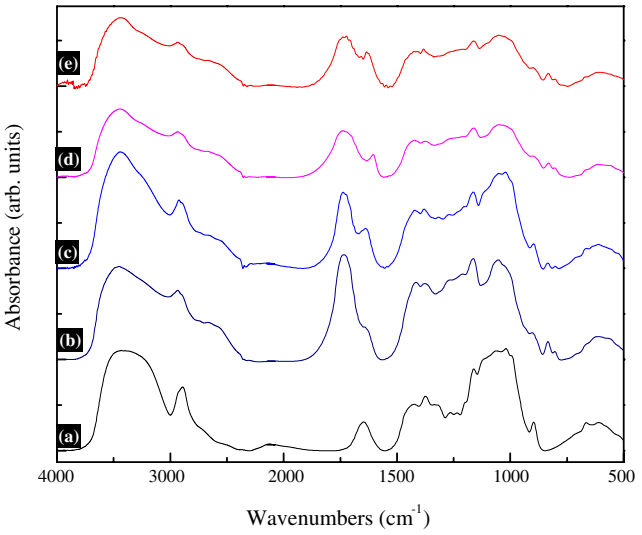

Figure 2. FT-IR spectra of (a) VR, (b) VRS, and VRS with trivalent metal ion complexes: (c) Cr^{3+} 1.48 mmol/g (d) Al^{3+} 1.05 mmol/g (e) Fe^{3+} 1.01 mmol/g.

of carboxyl appeared in the spectrum of the VRS and did not appear the spectrum of the VR. A broad and intense band in the 3000–3700 cm^{-1} region was assigned to free and hydrogen bonded OH stretching vibration of the VR. Due to carboxylic acid dimers in the VRS, the broad band was extended to 2400 cm^{-1} and exhibited more intense in the region of 3150–2400 cm^{-1}. The asymmetric CH_2 stretching vibration for the VR appeared near 2891 cm^{-1}. The VRS were characterized by the absorption of a symmetrical band around 2930 cm^{-1} that was attributable to CH_2 groups and this band was shifted to higher wavelength from 2891 cm^{-1} which was assigned to CH_2 on the VR.[18] It might be elucidated that CH_2 groups of succinic group on the VRS may be presented as indicative of CH_2 on aliphatic group which was observed near 2930 cm^{-1}. A band appeared at 834 cm^{-1} was assigned to wagging (out of plane bending) vibrations of carboxyl groups of the VRS.

Water absorption in the VR was observed at 1644 cm^{-1}. In the spectrum of the VRS, very strong peaks carboxyl and carbonyl were appeared at 1734 cm^{-1} which is attributed to C=O stretching bands. The peak at 1163 cm^{-1} attributed to C-O stretching in the esters (O-(C=O)$CHCH_2$) on the VRS were overlapped on the peak at 1160 cm^{-1} that was exhibited on the VR.

The FT-IR spectra of Al, Fe, and Cr adsorbed on the VRS were carried out as shown Figure 2. In the investigation of all metal adsorptions, the spectra reveal the presence of coordinated water molecules that indicated by broad bands at 3400–3465 cm^{-1}. This peak was attributed to stretching vibrations of the OH groups of water molecules. When the metal complexes were derived from carboxylic acids and metal ions, the C=O and C-O were replaced by two equivalent carbon–oxygen bonds which are intermediate in force constant between the C=O and C-O. The intensities of dimer bonding, which took place at 2400–3200 cm^{-1}, were decreased due to complexation of metal adsorption of VRS. These bonds were strongly

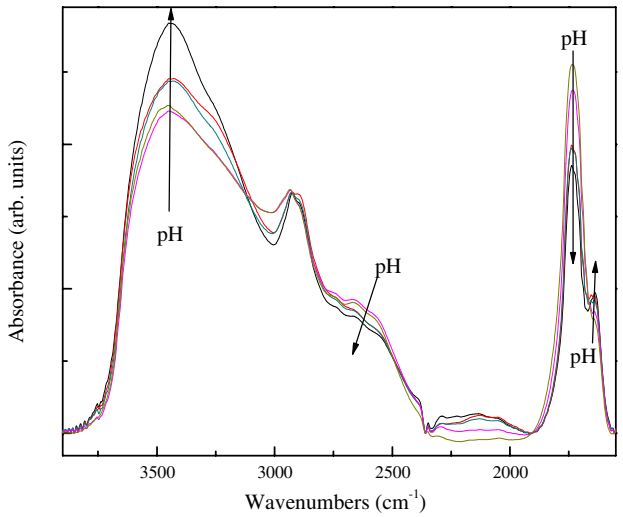

Figure 3. The comparison of FT-IR spectra of VRS Cr^{3+} increasing pH.

coupled resulting in strong asymmetric CO_2 stretching vibrations at 1605 cm^{-1}, 1635 cm^{-1}, and 1639 cm^{-1} which were corresponded to carboxyl ion groups with metals such as Al^{3+}, Fe^{3+}, and Cr^{3+}, respectively. Therefore, these peaks were shifted to lower wavelength than the peak of original carboxyl groups due to the bonds between carboxyl groups and metals that could reduce to double bonding property of carbonyl groups and caused to weaken the frequency of the double bond.

FT-IR Study on Cr^{3+} with Various pHs

Figure 3 shows the FT-IR spectra of Cr^{3+} adsorbed on the VRS with increasing pH. The intensity of the broad band at 2400–3200 cm^{-1}, which was associated with carboxylic acid dimers, decreased when the amount of metal ions adsorbed on the VRS increased. Moreover, it is interesting that an intensity of broad band in the region from 3600 cm^{-1} to 3100 cm^{-1} increased with rising pH. It might be dealt with that the amount of hydrate bonding depended on adsorbed metal ions on the VRS. Since the alteration peak of COOH is a useful indicator for monitoring the organizational changes of metal adsorption. It can be seen in Figure 3 that some COOH, which peaked at 1739 cm^{-1}, switched to COO^- which peaked at 1639 cm^{-1}. Therefore, the intensity of the peak at 1739 cm^{-1} decreased. By contrast, as pH decreased, the intensity of the peak occurring at 1739 cm^{-1} (COOH) increased due to the switching of fewer ionic bonds between COO^- and Cr^{3+}.

SEM images in Figure 4 show (a) the VRS-Al and the corresponding (b) Al mapping images by EDS. Figure 4(a) shows a typical the VR image. The mapping of aluminum Figure 4(b) shows that the elements, within the magnification used, are well dispersed on the matrix surface. The Al emission line, observable as white dots, is at 1.475 keV.[19] In the SEM images, no degradation was observed on fiber type of VRS-Al after synthesizing VRS. Fiber type ion exchanger and chelating agents have the high specific surface areas that contribute to the much higher adsorption rate and adsorption capacity of fibrous agents than resin type of ion exchanger.[12]

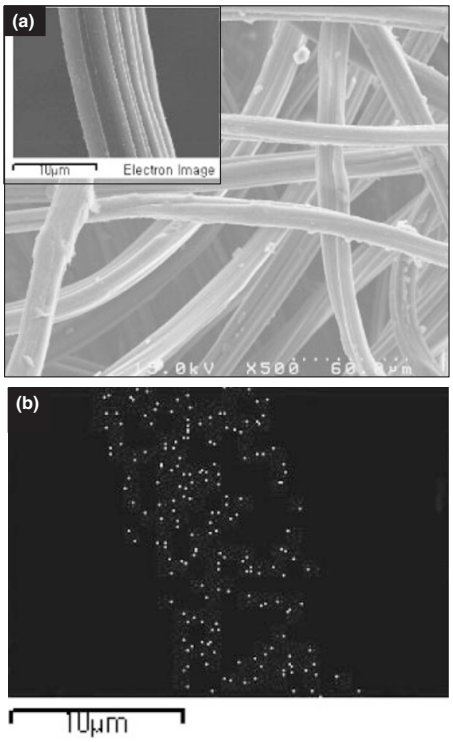

Figure 4. SEM images of (a) VRS-Al and the corresponding EDS Al mapping image (b). The Al emission line appears as white points.

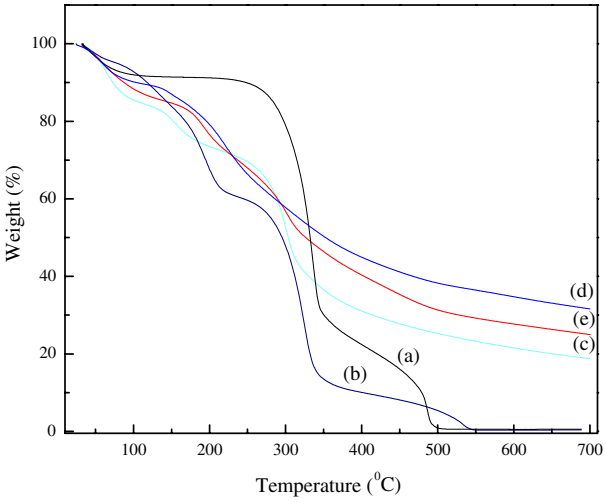

Figure 5. TGA curves of (a) VR, (b) VRS, and VRS with metals (c) VRS-Al, (d) VRS-Fe, and (e) VRS-Cr.

Studies of Thermal Properties

Figure 5 shows TGA curves of modified viscose rayons. TGA curves were obtained under a nitrogen atmosphere at a heating rate of 10 °C/min. The TGA curve of the VR shows two main steps of weight loss behavior. The first weight loss occurred at 90 °C. This weight loss was caused by the volatilization of volatile matter and/or the evaporation of residual absorbed moisture. For viscose rayon, dehydration was taken place in a temperature range of 90–270 °C, thermal degradation occurred rapidly at 270 °C, and char was formed at

343 °C. However, this char was not an original felt form. Most of the viscose rayon degraded at this temperature. In the case of the VRS, thermal degradation could be divided into three steps. First step was as if the first step of other samples. But the second step of weight loss occurred right after the first step because of the dehydration of the viscose rayon and it ended at 212 °C. The presence of the succinic groups on the VR influenced thermostability of the VR to be decreased. It was probably forced by the liquid matrix of dehydration of succinic group, which is derived above 105 °C and higher melting point of succinic acid around 200 °C causes to decompose with melting.[20] Third step started at 247 °C and ended 341 °C and represented the main thermal degradation of the viscose rayon succinate chains. Since the third step, the carbonization of the products was derived to ash.

Figure 5 also shows TGA curves of VRS metal complexes such as (c) VRS-Al, (d) VRS-Fe, and (e) VRS-Cr as well. Dehydration step of the VRS metal complexes might absorb some extent of heat and the melting temperature of succinic group was occurred at 95 °C. After dehydration step, a metal complex was decomposed at the temperature range of 95–287 °C with similar of each others. Char formation step of thermal degradation did not occur rapidly. The VRS metal complexes with Al, Fe, and Cr showed 19%, 25%, and 31% of ash formation at 700 °C, respectively. It is considered that not only the boundaries of the three steps depended on the nature of the complexes but also concentration of metals in VRS metal complexes. Metal hydrates were thought to decompose into its constituents, with the absorption of heat.[21] Therefore, heat transfer to the portion near the metals in VRS complexes is reduced even though temperature is increasing. The contents of metals in VRS metal complexes were as followed: 1.029 mmol of Fe, 1.059 mmol of Al and 1.48 mmol of Cr in 1 g of VRS-Fe, VRS-Al and VRS-Cr, respectively. The shape of thermal degradations of VRS metal complexes was different as observed in Figure 5 due to the fact that the amounts of metals in VRS metal complexes were not same as each other. In the case of the VRS-Fe and VRS-Al, the difference of metal contents was negligible (0.03 mmol/g). However, the ash residue of VRS-Fe is higher than the ash residue of VRS-Al because of the difference between atomic weight of Fe and Al (the atomic weight of Fe is more than double of the Al).

Study on Quantitative Analysis of the Adsorption of Al^{3+}, Fe^{3+}, and Cr^{3+}

Figure 6 shows the quantitative analyses of trivalent metals adsorbed on the VRS with increasing pH. The difference in the curves might be explained by the inherent chemical and physical properties of heavy metal ions. As the pH increased, the behavior of the VRS showed a more pronounced reactivity with the metals. In an acid medium, the VRS was highly protonated, and this characteristic reduced the attracting effect of the metal ion due to the lack of negative charges. In particularly for the carboxyl groups, adsorption phenomenon can occur in spite of the p*K*a being higher than pH of the medium.[15] Metal adsorption was found to be significantly

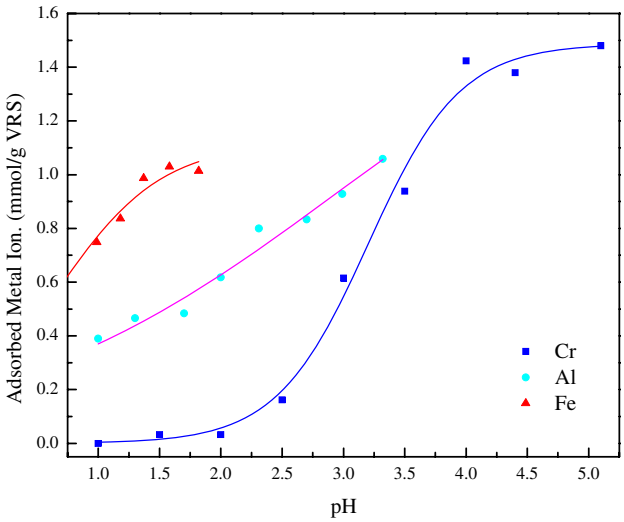

Figure 6. Experimental data and model plotting for cation adsorptions on VRS with increasing pH.

influenced by the solution pH. 1.48 mmol of Cr^{3+} in a 1 liter aqueous solution adsorbed on a gram of the VRS at pH 4 represented the maximum adsorption. As seen in Figure 6, the maximum adsorptions of metal ions can be ordered as $Cr^{3+} > Al^{3+} > Fe^{3+}$. However, at the same pH values, adsorptions of metal ions also classified as Fe^{3+}, Al^{3+}, and Cr^{3+}. The order of metal adsorption was determined by the methodology outlined in section 3.6 using the factors, $P(A)$, $K_{\text{effect.}}$, and χ which were obtained from the equilibrium model of each of the metal adsorptions.

Equilibrium Model for Cation Adsorption on the VRS

Equilibrium structural properties of solutions and the VRS which is randomly tangled polymer In the experimental data, not all carboxyl groups on the VRS were covered by the metal ions.

This indicates that adsorption depended on the interaction between the VRS, which consists of intrinsically flexible chains which stay flexible on small length scales, and the behavior of metal ions. In water, protons of carboxyl groups on the VRS dissociated and the carboxyl groups became ionized. This reaction demonstrates that the carboxylic ions can bond with metal ions to form a neutral species and establish equilibrium. This result can be described by the following chemical equilibriums:

$$\text{RCOOH} \leftrightarrow \text{RCOO}^- + \text{H}^+ \quad (1)$$

$$3\text{RCOO}^- + \text{Cr}^{3+} \leftrightarrow (\text{RCOO})_3\text{Cr} \quad (2)$$

Since we assume that both RCOO^- and $(\text{RCOO})_3\text{Cr}$ groups are confined to the surface, we carefully considered the entropy of the mixing contribution to the free energy.[22] The chemical potential of a surface group can be written as:

$$\mu_{\text{RCOO}^-} = \mu^{\theta}_{\text{RCOO}^-}(surface) + \mu_{\text{RCOO}^-}(entropy\ of\ mixing) + \mu^{el}_{\text{RCOO}^-}$$

If we assume a random (ideal) mixing of $RCOO^-$ and Cr^{3+} groups, the entropic term becomes

$$\mu_{RCOO^-}(entropy\ of\ mixing) = kT \ln X_{RCOO^-}$$

where

$$X_{RCOO^-} = \frac{3n_{RCOO^-}}{3n_{RCOO^-} + n_{(RCOO)_3Cr}}$$

Similarly, for the neutral RCOOH and $(RCOO)_3Cr$ groups with surface mole fraction X_{RCOOH} and $X_{(RCOO)_3Cr}$ we have:

$$\mu_{RCOOH} = \mu^{\theta}_{RCOOH}(surface) + kT \ln X_{RCOOH}$$
$$\mu_{(RCOO)_3Cr} = \mu^{\theta}_{(RCOO)_3Cr}(surface) + kT \ln X_{(RCOO)_3Cr}$$

The electrostatic contribution, $\mu^{el}_{RCOO^-}$, to the chemical potential of the charged surface group represents the free energy required to bring a charge $z_{RCOO^-}e$ from the bulk surface. This amounts to:

$$\mu^{el}_{RCOO^-} = z_{RCOO^-}e\Psi_0$$

The chemical potential of the ion H^+ and Cr^{3+} is uniform and assumes ideal solution behavior.

$$\mu_{H^+} = \mu^{\theta}_{H^+}(solution) + kT \ln C_{H^+}$$
$$\mu_{Cr^{3+}} = \mu^{\theta}_{Cr^{3+}}(solution) + kT \ln C_{Cr^{3+}}$$

By requiring that chemical potentials are equal for the left- and right-hand sides of equations 1 and 2, we obtain the following equilibrium equations:

$$\frac{X_{RCOOH}}{X_{RCOOH}C_{H^+}} = K'_{RCOO^-} \exp\left(\frac{z_{RCOO^-}e\Psi_0}{kT}\right)$$
$$\frac{X_{(RCOO)_3Cr}}{X^3_{RCOO^-}C_{Cr^{3+}}} = K''_{RCOO^-} \exp\left(\frac{z_{RCOO^-}e\Psi_0}{kT}\right)$$

where Ψ_0 is the surface potential, e is the elementary charge, z_{RCOO^-} is a valence, T is the temperature, k is the Boltzmann's constant,

$$X_{(RCOO)_2Cu} = \frac{n_{(RCOO)_3Cr}}{3n_{RCOO^-} + n_{(RCOO)_3Cr}},$$
$$kt \ln K'_{RCOO^-} = \mu^{\theta}_{H^+}(solution) + \mu^{\theta}_{RCOO^-}(surface) - \mu^{\theta}_{RCOOH}(surface) \quad \text{and}$$
$$kt \ln K''_{RCOO^-} = \mu^{\theta}_{Cr^{3+}}(solution) + \mu^{\theta}_{RCOO^-}(surface) - \mu^{\theta}_{(RCOO)_3Cr}(surface)$$

To obtain $X_{(RCOO)_3Cr}$, the effective concentration for n_{RCOO^-} is required.

Semidilute Polyelectrolyte Solutions. The configuration of a polyelectrolyte chain in a semidilute solution with added metal ions is shown in Figure 7. On sufficiently small length scales (less than the electrostatic blob size D), the polymer-solvent interactions of the g_e monomers in each electrostatic blob depend on solvent quality. In good and Θ solvent, the electrostatic interaction energy due to charge repulsion within an electrostatic blob is on the order of thermal energy.[23]

$$\left(\frac{g_e}{A}\right)^2 \frac{e^2}{\varepsilon D} \approx kT \quad T \geq \Theta \tag{3}$$

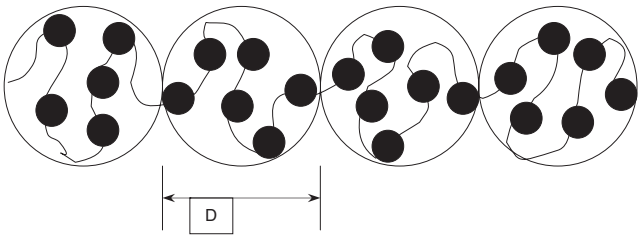

Figure 7. Polyelectrolyte conformation in semidilute solution: the chain of blobs.

Where A is the average number of monomers between uncondensed charges, e is the elementary charge, ε is the dielectric constant of the solvent, k is the Boltzmann constant, and T is the temperature.

Equation 3 can be simplified using the Bjerrum length $l_B = q^2/(\varepsilon kT)$. The Bjerrum length is the distance at which the energy of the Coulomb interaction between two elementary charges is equal to thermal energy.

$$\left(\frac{g_e}{A}\right)^2 l_B \approx D \quad T \geq \Theta \tag{4}$$

On the other hand, g_e has a certain amount of charges. The total concentration n_{RCOO^-} can be written as:

$$g_e = \vartheta' n_{RCOO^-} \tag{5}$$

where ϑ' is the proportional coefficient.

A is the number of monomers between effective charges and thus incorporates any effects of counterion condensation. Therefore, we can also write:

$$A = \vartheta'' n_{RCOO^-,effect} \tag{6}$$

where ϑ'' is the proportional coefficient, and $n_{RCOO^-,effect}$ is the effective concentration of n_{RCOO^-}.

The concentrations of n_{RCOO^-} in equation 5, and $n_{RCOO^-,effect}$ in equation 6, are substituted into equation 4.

$$\frac{n_{RCOO^-,effect}}{n_{RCOO^-}} = P(A); \quad \frac{\vartheta'}{\vartheta'' P(A)} \approx \sqrt{\frac{l_B}{D}};$$

where $P(A)$ is the probability factor. In the equilibrium and isotherm state of the system, we can assume that the Bjerrum length l_B is constant and the electrostatic blob size D is fixed. A value $P(A)$ will be in the range of $0 < P(A) \leq 1$.

Dissociation of Protons. Surfaces with acidic or basic functional groups undergo acid base reactions in aqueous media which lead to formation 1. In low surface potentials, the surface concentration of protons is commonly approximated by the Boltzmann distribution.[24] In order to fit the model on experiential data, we assumed the addition of a parameter χ into the approximation of the Boltzmann distribution as a degree of protonation:

$$C_{H^+,effect} = C^{\chi}_{H^+}{}^{*} \exp\left(-\frac{F\Psi_0}{RT}\right)$$

where $C_{H^+,effect}$ is the concentration of protons on the surface, C_{H^+} is the pH of the media and χ is the assumed degree of protonation ($0 < \chi \leq 1$).

Equilibrium Adsorption Concentration. By combining the equilibrium equation of the chemical potential of a surface group, theory of semidilute polyelectrolyte solutions, and the dissociation of protons from the VRS based on the Boltzmann distribution, we can write the equilibrium adsorption concentration as:

$$X_{(RCOO)_3Cr} = \frac{n_{(RCOO)_3Cr}}{3P(A)n_{RCOO^-} + n_{(RCOO)_3Cr}} = \frac{K''_{RCOO^-}}{K'^3_{RCOO^-}} \frac{1}{C^3_{H^+}} X^3_{RCOOH} C_{Cr^{3+}}$$

$$\frac{n_{(RCOO)_2Cu}}{3P(A)n_{RCOO^-} + n_{(RCOO)_3Cr}} = \frac{K_{effect}}{27} C_{Cr^{3+}} 10^{3\chi pH} \exp\left(\frac{2F\Psi_0}{RT}\right)$$

where

$$K_{effect} = \frac{K''_{RCOO^-}}{K'^2_{RCOO^-}}$$

$$n_{RCOO^-} = n_{RCOO^-.max} - 3n_{R(COO)_3Cr}$$

and

$$X_{RCOOH} = 1/2, \quad C_{Cr^{3+}} = 1 \times 10^{-2}\,\text{mol/L}$$

$$T = 293.45\,\text{K}$$

n_{RCOO^-} means moles of chelate groups that can combine with cations. Cr^{3+} ion can bond with two $RCOO^-$ groups. Therefore, $n_{RCOO^-.max} - 3n_{R(COO)_3Cr}$ is used for n_{RCOO^-}, and $n_{RCOO^-.max}$ (6.2 mmol) is the maximum metal ion adsorption mole on the VRS. This value is analogous to:

$$\frac{n_{(RCOO)_3Cr}}{3P(A)n_{RCOO^-max} - 9P(A)n_{(RCOO)_3Cr} + n_{(RCOO)_3Cr}} = \frac{K_{effect}}{27} C_{Cr^{3+}} 10^{3\chi pH} \exp\left(\frac{2F\Psi_0}{RT}\right)$$

We can also derive the same equilibrium model for other metal ions such as Al^{3+}, and Fe^3 with the same initial concentration value of metal ions as found in Cr^{3+}.

The Effects of the Factors $P(A)$, χ, and K_{effect} on Metal Adsorption

The factors and surface potentials of metal ion adsorption were obtained by equilibrium modeling using the empirical data shown in Figure 6 (curves). The probability factor $P(A)$ might represent how much carboxyl groups can be available to bond with metal ions. Accordingly, the probability factors of carboxyl groups of the VRS inverse with metal ions such as Al^{3+}, Cr^{3+}, and Fe^{3+} were found to be 0.1099, 0.10959, and 0.10909, respectively. Each of the values of $P(A)$ demonstrated the hindrance effect of the VRS that occurred due to the lack of effective carboxyl groups. Also, a degree of protonation was to assume protonation of the VRS in solution that could compete against metal ions adsorption. The degrees of protonation of each of adsorption obtained as $\chi = 0.10354$ (Al), $\chi = 0.33695$ (Fe), and $\chi = 0.38715$ (Cr). If a degree of protonation was low, it increased of available carboxyl groups. However, the effective ratio of surface equilibrium constants Cr^{3+} adsorption on the VRS, $K_{effect} = 0.03617$, caused the adsorption to decrease because the surface equilibrium constant for protonation was higher than for chromium ion. The effective ratio of Cr^{3+}, $K_{effect} = 0.03617$, was significantly lower compared to the factor of Al^{3+} $K_{effect} = 0.30952$, and Fe^{3+} $K_{effect} = 0.78282$. The significant difference between Cr^{3+} resulted in a lower adsorption of Zn^{2+} compared to Al^{3+} and Fe^{3+} in same pH values. The surface potential, Ψ_0, of the VRS for all metal adsorptions was -1.6296 mV since all metal ions were considered to react with the surface on the same surface plane.

CONCLUSIONS

This study was dealt with the investigation synthesized the VRS and its physico-chemical properties. The confirmation of structures of the VRS, the VRS metal complexes were performed by ^{13}C solid state NMR and FT-IR. The peaks corresponded to carboxyl groups at 1734 cm^{-1}, carboxyl groups with metals in the range of 1605–1639 cm^{-1} were certified FT-IR spectra after esterification, adsorption of metals, respectively. Thermal study was carried out by TGA that exhibited curves of weight loss of the samples with increasing temperature range of 30–700 °C. Weight residues of all the VRS metal complexes were increased compared to the VR and described in the following order: VRS-Cr > VRS-Fe > VRS-Al. The adsorption of metal on VRS increased when the pH increased. The maximum metal ions adsorbed could be classified as $Cr^{3+} > Al^{3+} > Fe^{3+}$. In order to predict adsorption and the order of metals on the VRS, an equilibrium model was modified using basic chemical potentials and the Boltzmann distribution. The probability factor $P(A)$, the degree of protonation χ, the effective ratio of the surface equilibrium constants K_{effect}, and the surface potential Ψ_0, were calculated by inserting them in a model that fit the experimental data. These factors well demonstrated the adsorption capacity of metals on the VRS. The most effective indicator was the probability factor because it clearly predicted how much carboxyl groups on the VRS were available to bond with the metal ions.

NOMENCLATURE

A	number of monomers between uncondensed charges
C_i	concentration of component i (mol)
D	electrostatic blob size
e	elementary charge (C)
F	Faraday constant (C/mol)
g_e	number of monomers in an electrostatic blob
k	Boltsmann constant (J/K)
K'_i, K''_i	surface equilibrium constant
K_{effect}	effective ratio of surface equilibrium constants $\left(= \frac{K''_{RCOO^-}}{K'^2_{RCOO^-}}\right)$
l_B	Bjerrum length
M	mass of the VRS (g)
n_i	mole of component i (mmol)
q_e,	cation exchange capacity (meq/g)
R	shown in Fig. 1
R	ideal gas constant (J/Kmol)

T temperature (K)
V_{25} volume sampled from the solution (dm^3)
V_{100} volume of the solution (dm^3)
V_{HCl} volume of HCl for back titration (dm^3)
X_i mole fraction of component i
z_i valency of component i
χ degree of protonation
ε dielectric constant
$P(A)$ probability factor
ϑ', ϑ'' proportional coefficient
μ_i chemical potential of component i
μ_i^{el} chemical potential of component i considering the electrostatic contribution
μ_i^{θ} chemical potential of component i in the standard state
Θ theta temperature
Ψ_0 surface potential (mV)

Received: September 4, 2007
Accepted: December 17, 2007
Published: February 26, 2008

REFERENCES

1. V. Vuorio, J. A. Manzanares, L. Murtomaki, J. Hirvonen, T. Kankkunen, and K. Kontturi, *J. Controlled Release*, **91**, 439 (2003).
2. O. A. El Seoud and T. Heinze, *Adv. Polym. Sci.*, **186**, 103 (2005).
3. K. J. Edgar, C. M. Buchanan, J. S. Debenham, P. A. Rundquist, B. D. Seiler, M. C. Shelton, and D. Tindall, *Prog. Polym. Sci.*, **26**, 1605 (2001).
4. W. M. Hosny, *Polym. Int.*, **42**, 157 (1997).
5. T. W. Swaddle, J. Rosenqvist, P. Yu, E. Bylaska, B. L. Phillips, and W. H. Casey, *Science*, **308**, 1450 (2005).
6. M. A. S. D. Barros, A. S. Zola, P. A. Arroyo, C. R. G. Tavares, and E. F. Sousa-Aguiar, *Adsorption*, **12**, 239 (2006).
7. C. W. MacDiarmid and R. C. Gardner, *J. Biol. Chem.*, **273**, 1727 (1998).
8. H. Jacqmin, D. Commenges, L. Letenneur, P. Barberger-Gateau, and J.-F. Dartigues, *Am. J. Epidemiol.*, **139**, 48 (1994).
9. S. Lacour, V. Deluchat, J.-C. Bollinger, and S. Bernard, *Talanta*, **46**, 999 (1998).
10. P. M. Outridge and A. M. Scheuhammer, *Rev. Environ. Contam. Toxicol.*, **130**, 31 (1993).
11. W. N. Harrison, S. M. Bradberry, and J. A. Vale, *Clinical Toxicology*, **38**, 137 (2000).
12. W. Lin and Y. L. Hsieh, *Ind. Eng. Chem. Res.*, **35**, 3817 (1996).
13. F. Beolchini, F. Pagnanelli, L. Toro, and F. Veglio, *Water Res.*, **40**, 144 (2006).
14. Z. Reddad, C. Gerente, Y. Andres, and P. L. Cloirec, *Environ. Sci. Technol.*, **36**, 2067 (2002).
15. A. Esposito, F. Pagnanelli, and F. Veglio, *Chem. Eng. Sci.*, **57**, 307 (2002).
16. J. Peydecastaing, S. Girardeau, C. Vaca-Garcia, and M. Borredon, *Cellulose*, **13**, 95 (2006).
17. H. Yuksek, M. Alkan, S. Bahceci, I. Cakmak, Z. Ocak, H. Baykara, O. Aktas, and E. Agyel, *J. Mol. Struct.*, **873** 142 (2008).
18. N. B. Colthup, L. H. Daly, and S. E. Wiberley, "Introduction to Infrared and Raman Spectroscopy," Academic Press Inc, London, 1964.
19. R. V. S. Alfaya and Y. Gushikem, *J. Colloid Interface Sci.*, **213**, 438 (1999).
20. A. A. M. A. Nada and M. L. Hassan, *J. Appl. Polym. Sci.*, **102**, 1399 (2006).
21. Y. G. Ko, U. S. Choi, B. G. Ahn, and D. J. Ahn, *J. Polym. Sci., Part A: Polym. Chem.*, **38**, 2815 (2000).
22. D. F. Evans and H. Wennerstrom, "The Colloidal Domain: Where Physics, Chemistry, Biology, and Technology Meet," 2nd ed., Wiley, New York, 1999, p 127.
23. A. V. Dobrynin, R. H. Colby, and M. Rubinstein, *Macromolecules*, **28**, 1859 (1995).
24. R. Schweiss, P. B. Welzel, C. Werner, and W. Knoll, *Langmuir*, **17**, 4304 (2001).